ChemComm

COMMUNICATION

View Article Online
View Journal | View Issue

Cite this: *Chem. Commun.*, 2016, 52, 3927

Received 29th October 2015,
Accepted 5th February 2016

DOI: 10.1039/c5cc08978f

www.rsc.org/chemcomm

Tuning the surface structure of supported $PtNi_x$ bimetallic electrocatalysts for the methanol electro-oxidation reaction†

Bingsen Zhang,*[a] Yiming Niu,[a] Junyuan Xu,[a] Xiaoli Pan,[a] Cheng-Meng Chen,[b] Wen Shi,[a] Marc-Georg Willinger,[c] Robert Schlögl[c] and Dang Sheng Su*[a]

The structures of $PtNi_x$ nanoalloy particles were modified through thermal annealing in different atmospheres. The evolution of surface structures was uncovered by advanced transmission electron microscopy, and the structure–function correlation in methanol electro-oxidation was probed. It provided new insights into the design and synthesis of highly efficient electrocatalysts.

Nowadays, fuel cells have attracted extensive interest in the search for a solution to energy shortage and environmental pollution.[1–3] Direct methanol fuel cells (DMFCs) have become increasingly important because of their low cost, high-efficiency energy conversion, less pollution and safe storage as well as transport.[4] Platinum (Pt) as the most generally accepted active metal for the cathode electrode material[5] plays a very important role in fuel cells, but the high cost and poor stability limit its application. The introduction of other metal elements, especially the low-cost 3d transition metals (*e.g.* Fe, Co and Ni), not only reduces the usage of Pt, but also modifies the electronic and chemical properties, which could result in enhanced electrocatalytic activity.[6–10] It has been traced and illustrated that electrocatalytic reactions take place on the surface of catalysts,[11,12] where adsorption and desorption occur. Therefore, the activity of electrocatalysts highly depends on their surface properties,[13] and higher catalytic activity can be obtained by tuning the surface structure and the composition of Pt-based nanomaterials.[14,15] In order to control the surface structure and composition at the atomic scale, various methods have been developed, including multistep synthesis[16] and electrochemical dealloying.[17–19] For instance, Stamenkovic *et al.* designed and synthesized a novel Pt_3Ni catalyst for the oxygen reduction reaction (ORR).[1] The outermost layer and the second atomic layer of Pt_3Ni nanoparticles (NPs) are Pt-rich and Ni-rich, respectively, and the weak interaction between them makes the $Pt_3Ni(111)$ more active. However, there are few reports regarding the surface/interface structural evolution induced by thermal annealing in different atmospheres on Pt-based nanoalloy NPs in detail, although it is significant for a more precise and easy control of the fine structures of catalysts.[20–24] Thanks to the developments in transmission electron microscopy (TEM), by which the structural investigation of the solid catalyst at the atomic level becomes possible during the synthesis process and catalysis reaction.[25,26]

Herein, the polyhedral $PtNi_2$ NPs synthesized using a solvothermal method were supported on multilayer graphene ($PtNi_2$/Gr), and then $PtNi_2$/Gr was thermally annealed in a distinct atmosphere. The carbon monoxide (CO)-induced surface reconstruction of the polyhedral $PtNi_2$ NPs led to a core–shell structure with a Pt-rich surface. The methanol electro-oxidation was selected as the probing reaction for testing the performance of $PtNi_2$ nanoalloy NPs with different structures. The results indicate that the interaction between CO and the metal (Pt and Ni) during the thermal treatment provides a facile approach to tune the surface structure of the $PtNi_2$ catalyst.

Fig. 1 shows representative low-magnification TEM images of $PtNi_2$ NPs. The particle size distribution (PSD) of $PtNi_2$ NPs is from 5.4 nm to 12.6 nm, and the average size is *ca.* 9.6 nm based

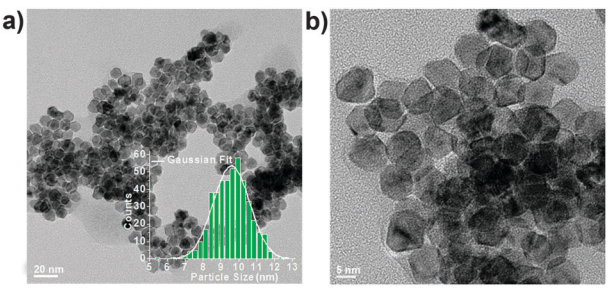

Fig. 1 Representative TEM images of $PtNi_2$ NPs before supporting. The inset in (a) is the corresponding particle size distribution.

[a] *Shenyang National Laboratory for Materials Science, Institute of Metal Research, Chinese Academy of Sciences, 72 Wenhua Road, Shenyang, 110016, China. E-mail: bszhang@imr.ac.cn, dssu@imr.ac.cn*
[b] *Key Laboratory of Carbon Materials, Institute of Coal Chemistry, Chinese Academy of Sciences, 27 Taoyuan South Road, Taiyuan, 030001, China*
[c] *Fritz Haber Institute of the Max Planck Society, Faradayweg 4–6, Berlin, 14195, Germany*

† Electronic supplementary information (ESI) available: Experimental procedures and characterization data. See DOI: 10.1039/c5cc08978f

on the statistical analysis of the PSD histogram (the inset in Fig. 1a). Subsequently, the synthesized $PtNi_2$ NPs were supported on multilayer graphene. The obtained supported $PtNi_2$ NPs were heated to 300 °C for 4 hours in argon (Ar) and CO gases, named as $PtNi_2$/Gr–Ar and $PtNi_2$/Gr–CO, respectively.

X-ray diffraction (XRD) patterns (Fig. S1, ESI†) show that all of the $PtNi_2$ catalysts exhibit face-centred cubic structures, without a single Pt or Ni phase. The characteristic diffraction peaks of $PtNi_2$ NPs between Pt and Ni diffraction-peak positions can be indexed (111), (200) and (220) peaks based on JCPDS cards of Pt (No. 04-0802) and Ni (No. 04-0850). The full-width half-maximum (FWHM) values of (111), (200) and (220) peaks decrease after thermal treatment, indicating an increase in the crystallinity of $PtNi_2$ NPs. The main peaks of $PtNi_2$/Gr–CO shift toward a higher angle (Ni phase) compared with that of $PtNi_2$/Gr, which indicates that some Pt atoms segregate and the other Pt and Ni atoms form the $PtNi_x$ ($x > 2$) nanoalloy.

Advanced electron microscopy techniques were used for uncovering the shape, composition and fine structures of the supported $PtNi_2$ NPs. The $PtNi_2$ NPs are highly dispersive on the multilayer graphene in the $PtNi_2$–Gr sample, as shown in the high-angle annular dark field-scanning transmission electron microscopy (HAADF-STEM) image (Fig. 2a). High-resolution TEM (HRTEM) observations reveal that the shape of $PtNi_2$ NPs is polyhedral (Fig. 2b). The lattice fringes (200) and (111), *d*-spacing 1.90 Å and 2.12 Å, of $PtNi_2$ with a characteristic acute angle of 53.7° were identified on the NPs, referring to the JCPDS cards (Pt: No. 04-0802, Ni: No. 04-0850, space group: $Fm\bar{3}m$). Summarizing the analyses of HRTEM images, the exposed facets of $PtNi_2$ NPs can be identified as the {002}, {111} and {220} planes (see the insets in Fig. 2b). However, only a few $PtNi_2$ NPs with good crystallinity exist in $PtNi_2$/Gr, and most of $PtNi_2$ NPs are polycrystalline with the size of the constituent single crystalline domains in the range between 1.0 and 8.0 nm, as shown in the colored HRTEM images (Fig. 2c and d). It is consistent with the XRD pattern that the diffraction peaks with the broad FWHM values in Fig. S1 (ESI†). According to above structural information, a structural model was proposed, showing the random distributions of Pt and Ni in most of polycrystalline $PtNi_2$ NPs (the lower-right inset in Fig. 2d).

Aiming to modify the surface structure of $PtNi_2$ NPs, the $PtNi_2$/Gr sample was thermally treated (300 °C) in Ar and CO gases. Fig. 3 shows the microscopic features of the $PtNi_2$/Gr sample treated in Ar gas. The $PtNi_2$ NPs remained highly dispersed on the supports except for slight agglomeration (Fig. 3a and Fig. S3a, ESI†). Most of $PtNi_2$ particles were rearranged to polyhedral NPs with good crystallinity, which has been identified by HRTEM (Fig. 3b and Fig. S3b, ESI†). According to HRTEM analyses, the $PtNi_2$ NPs are also encapsulated by the {002}, {111} and {220} planes (the inset in Fig. 3b). Moreover, there are some multiply twinned NPs in the $PtNi_2$/Gr–Ar, displayed in Fig. 3e and f. This result is in accordance with the XRD results that the FWHM value of diffraction peaks decreased slightly compared with that before annealing. EDS elemental maps show the distributions of Pt and Ni are uniform in $PtNi_2$ NPs (Fig. 3c and Fig. S3c, S5a, ESI†),

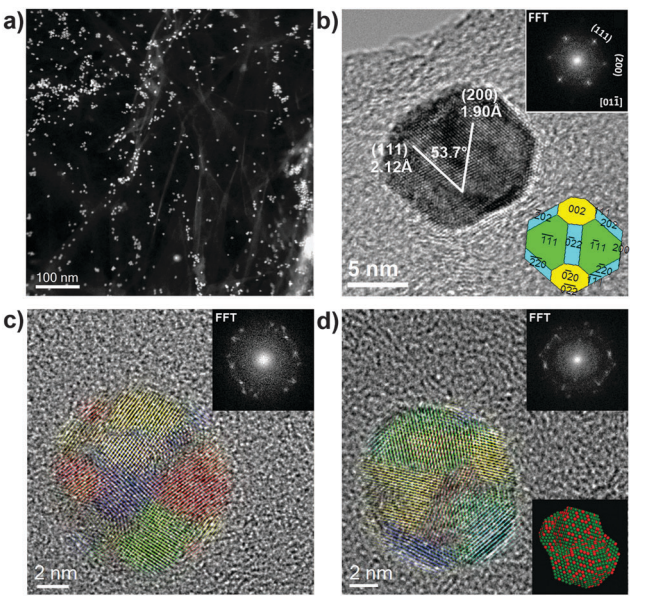

Fig. 2 Low-magnification HAADF-STEM image of $PtNi_2$/Gr (a), HRTEM images of polyhedral $PtNi_2$ NPs with good crystallinity (b), and polycrystalline $PtNi_2$ NPs (c and d). The top-right insets in (b–d) are the corresponding local Fast Fourier Transformation (FFT), and the lower-right insets in (b and d) are the shape and relevant atomic model (Pt-green, Ni-red) of $PtNi_2$ NPs. The constituent single-crystalline domains are indicated in different colours in (c) and (d).

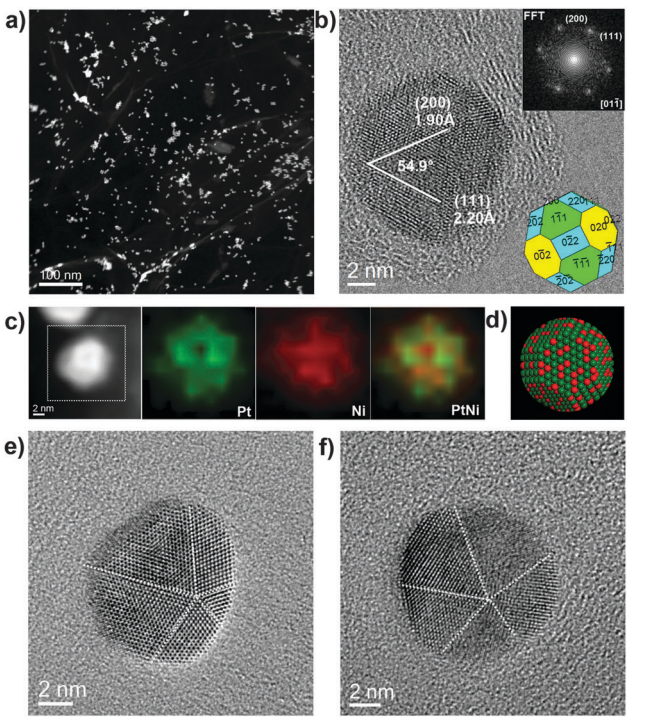

Fig. 3 Low-magnification HAADF-STEM image of $PtNi_2$/Gr–Ar (a), HRTEM images of polyhedral $PtNi_2$ NPs with good crystallinity (b), multiply twinned $PtNi_2$ NPs (e and f), EDS elemental maps (c) and relevant atomic models of $PtNi_2$ NPs (d: Pt-green, Ni-red). The insets in (b) are the corresponding local FFT and shape of the $PtNi_2$ NPs. The dashed white lines in (e) and (f) are the twin boundaries.

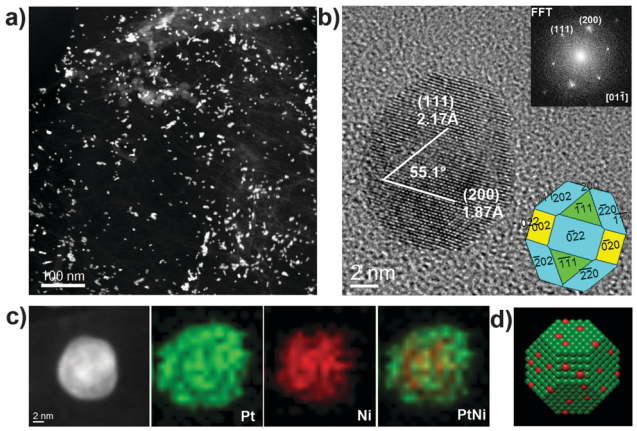

Fig. 4 Low-magnification HAADF-STEM image of $PtNi_2$/Gr–CO (a), HRTEM image of $PtNi_2$ NP (b), EDS elemental maps (c) and relevant atomic model (d: Pt-green, Ni-red) of $PtNi_2$ NPs. The insets in (b) are the corresponding local FFT and shape of $PtNi_2$ NP.

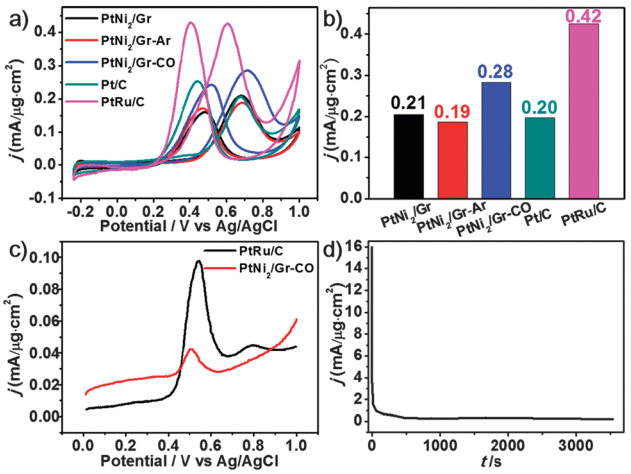

Fig. 5 (a) CV curves of $PtNi_2$-based catalysts PtRu/C and Pt/C in N_2-saturated 0.5 M H_2SO_4 + 2 M CH_3OH solutions at a scan rate of 50 mV s^{-1}. (b) The normalized current density histogram at the respective peak potential for all catalysts. (c) CO-stripping voltammograms at 50 mV s^{-1} of $PtNi_2$/Gr–CO and commercial PtRu/C (20 wt% Pt, 10 wt% Ru, Alfa Aesar) catalysts in 0.5 M H_2SO_4. (d) Chronoamperometric curve of MOR at 0.7 V on the $PtNi_2$/Gr–CO catalyst.

indicating the Pt and Ni rearranged and formed a randomly mixed bimetallic type after thermal annealing in Ar gas. The atomic model is shown in Fig. 3d, displaying a three-dimensional structure with a random distribution of Pt and Ni in $PtNi_2$ NPs.

The structures of the $PtNi_2$/Gr treated in CO gas exhibited distinct changes. Low-magnification (S)TEM images show that the $PtNi_2$ NPs are well distributed on the supports (Fig. 4a and Fig. S4a, ESI†). HRTEM reveals that all of the $PtNi_2$ NPs retain the polyhedral shape with exposed {002}, {111} and {220} facets, as shown in Fig. 4b and Fig. S4b (ESI†). On these exposed planes, there exists some surface roughness (*e.g.* corner and step defects), ascribed to the atom migration induced by the CO thermal annealing. These NPs are of good crystallinity. Furthermore, EDS elemental mapping reveals that the Pt element is enriched on the surface of $PtNi_2$ NPs, which formed the core ($PtNi_x$, $x > 2$)–shell (Pt) type (Fig. 4c and Fig. S4d, S5b, ESI†). The HR-STEM image in Fig. S4c (ESI†) clearly displays that brighter atoms (Pt) surround the Ni atoms, indicating a core–shell structure. Comparing the fine structures of $PtNi_2$ NPs treated with thermal annealing in different gases, the shapes and surface structures of $PtNi_2$ NPs can be tuned at the atomic level. Except for the microscopic features mentioned above, the composition of the serials of $PtNi_2$ samples has been characterized by inductively coupled plasma mass spectrometry (ICP-MS) (Table S1, ESI†). The composition of the $PtNi_x$ nanoalloy was kept nearly the same (the Pt/Ni atomic ratio was about 1/2) at the macroscopic scale.

For studying the effects of the tuned microstructures and for illustrating the structure–function relationship, the methanol electro-oxidation reaction (MOR) was selected as the probing experiment. The MOR performance on $PtNi_2$-based samples, PtRu/C and Pt/C was evaluated by cyclic voltammetry (CV) curves (Fig. 5a), and the normalized activity (current density) at the respective peak potential is shown in Fig. 5b. The better activity with 33% and 47% enhancement is presented in the $PtNi_2$/Gr–CO, compared to those of other two $PtNi_2$-based catalysts. The enhanced activity of the $PtNi_2$/Gr–CO sample can be attributed to the rearrangement of Pt and Ni induced by the CO thermal treatment and the much more amount of Pt atoms segregating on the surface.[11,27,28] The obtained best performance of the $PtNi_2$-based catalysts is between those of PtRu/C and Pt/C, which is also comparable to other PtNi-based catalysts reported previously.[29,30] The good CO tolerance of the $PtNi_2$-based samples are represented by the ratio (1.1–1.3) of forward (I_f) and backward (I_b) peak currents.[31] The CO-stripping of the $PtNi_2$/Gr–CO sample was also investigated compared to that of the commercial PtRu/C catalyst. From the lower current density and peak potential, it could be observed that the $PtNi_2$/Gr–CO sample shows a smaller amount of adsorbed CO and weaker CO adsorption on the surface during the electrocatalytic reaction than that of the commercial PtRu/C catalyst. In this case, the enhancement of CO tolerance can be explained by the electronic effect mechanism and the formation of Pt-rich shells.[29,30] The transition metal Ni changes the electronic properties of the $PtNi_x$ NPs *via* electron transfer between the Pt and Ni, which weakens the Pt–CO bond and suppresses the CO adsorption on the Pt rich surface. As for the stability, the MOR current density after 3000 s was also about 0.20, which is little lower than that of the 0.28 (Fig. 5a), as shown in Fig. 5d.

Several factors determine the surface segregation of the core–shell structure, which has been unravelled and interpreted based on experimental and theoretical studies,[32–38] such as cohesive energy, surface energy, atomic radius and electronegativity. The surface segregation energy (SE) is the main driving force for the formation of core–shell structures.[39] For instance, according to density functional theory (DFT) calculation, the SE of the 55-atom Ni-core and Pt-shell model is 0.42 eV. The core (Ni)–shell (Pt) structure is preferred when SE is positive, which is dominated by the smaller Wigner Seitz radius of Ni. It means that the compressive strain was relieved while the smaller atom goes into the core. This explanation is also supported by some related investigations.[40–43] In this work, CO molecules play a principal

role in the surface rearrangement. Based on the different CO adsorption energies (E_{ad}) on Pt(111) and Ni(111) calculated by DFT,[42] a reduction surface energy of about 0.67 eV per Pt atom rearranged to the surface was observed. Therefore, the segregation of Pt atoms is favourable during the thermal treatment in the CO surrounding. However, this phenomenon is not obvious in Ar gas due to the inert environment. Otherwise, the CO molecules adsorbed on the $PtNi_2$ NPs surface can restrain the shape change and retain the polyhedral morphology.[44,45]

In summary, we present a method to obtain a Pt-rich shell structure of $PtNi_2$ NPs supported on a multilayer graphene that retains the polyhedral shape with exposed {002}, {111} and {220} facets, which exhibits a better activity due to electronic and geometric effects in the MOR. Advanced electron microscopy unambiguously identified the structure evolutions of $PtNi_2$ NPs from polycrystalline materials to randomly mixed and core–shell bimetallic structures induced by thermal annealing in Ar and CO gases. It offers a good example on the investigation of the structural evolution of bimetallic systems modified by different approaches, and reveals the structure–function correlation in chemical reactions. This work also provides a new insight into the interaction between CO molecules and metals, which could further help in the design of high activity nanoalloy catalysts by precisely tuning the shape, structure and composition.

We gratefully acknowledge the financial support provided by the National Natural Science Foundation of China (91545119, 21203215, 21133010, 51221264, and 21261160487), the Youth Innovation Promotion Association CAS (2015152), China Scholarship Council (PPP: [2014]6013) and ''Strategic Priority Research Program'' of the Chinese Academy of Sciences (XDA09030103). Dr G.-R. Zhang and Dr Y. Zhu are gratefully acknowledged for their stimulating discussions.

Notes and references

1 V. R. Stamenkovic, B. Fowler, B. S. Mun, G. Wang, P. N. Ross, C. A. Lucas and N. M. Marković, *Science*, 2007, **315**, 493–497.
2 R. R. Adzic, J. Zhang, K. Sasaki, M. B. Vukmirovic, M. Shao, J. X. Wang, A. U. Nilekar, M. Mavrikakis, J. A. Valerio and F. Uribe, *Top. Catal.*, 2007, **46**, 249–262.
3 J. Liu, L. Jiang, Q. Tang, B. Zhang, D. S. Su, S. Wang and G. Sun, *ChemSusChem*, 2012, **5**, 2315–2318.
4 A. S. Aricò, S. Srinivasan and V. Antonucci, *Fuel Cells*, 2001, **1**, 133–161.
5 N. A. Hampson, M. J. Willars and B. D. McNicol, *J. Chem. Soc., Faraday Trans. 1*, 1979, **75**, 2535–2543.
6 D. F. van der Vliet, C. Wang, D. Tripkovic, D. Strmcnik, X. F. Zhang, M. K. Debe, R. T. Atanasoski, N. M. Markovic and V. R. Stamenkovic, *Nat. Mater.*, 2012, **11**, 1051–1058.
7 D. F. van der Vliet, C. Wang, D. Li, A. P. Paulikas, J. Greeley, R. B. Rankin, D. Strmcnik, D. Tripkovic, N. M. Markovic and V. R. Stamenkovic, *Angew. Chem., Int. Ed.*, 2012, **51**, 3139–3142.
8 S. Guo, S. Zhang and S. Sun, *Angew. Chem., Int. Ed.*, 2013, **52**, 8526–8544.
9 S.-I. Choi, M. Shao, N. Lu, A. Ruditskiy, H.-C. Peng, J. Park, S. Guerrero, J. Wang, M. J. Kim and Y. Xia, *ACS Nano*, 2014, **8**, 10363–10371.
10 R. Loukrakpam, J. Luo, T. He, Y. Chen, Z. Xu, P. N. Njoki, B. N. Wanjala, B. Fang, D. Mott, J. Yin, J. Klar, B. Powell and C.-J. Zhong, *J. Phys. Chem. C*, 2011, **115**, 1682–1694.
11 L. Gan, R. Yu, J. Luo, Z. Cheng and J. Zhu, *J. Phys. Chem. Lett.*, 2012, **3**, 934–938.
12 L. Gan, C. Cui, M. Heggen, F. Dionigi, S. Rudi and P. Strasser, *Science*, 2014, **346**, 1502–1506.
13 W. Yu, M. D. Porosoff and J. G. Chen, *Chem. Rev.*, 2012, **112**, 5780–5817.
14 V. Stamenkovic, B. S. Mun, K. J. J. Mayrhofer, P. N. Ross, N. M. Markovic, J. Rossmeisl, J. Greeley and J. K. Nørskov, *Angew. Chem., Int. Ed.*, 2006, **45**, 2897–2901.
15 V. R. Stamenkovic, B. S. Mun, K. J. J. Mayrhofer, P. N. Ross and N. M. Markovic, *J. Am. Chem. Soc.*, 2006, **128**, 8813–8819.
16 Z. Xu, Y. Hou and S. Sun, *J. Am. Chem. Soc.*, 2007, **129**, 8698–8699.
17 J. Erlebacher, M. J. Aziz, A. Karma, N. Dimitrov and K. Sieradzki, *Nature*, 2001, **410**, 450–453.
18 L. Gan, M. Heggen, R. O'Malley, B. Theobald and P. Strasser, *Nano Lett.*, 2013, **13**, 1131–1138.
19 D. Wang, Y. Yu, H. L. Xin, R. Hovden, P. Ercius, J. A. Mundy, H. Chen, J. H. Richard, D. A. Muller, F. J. DiSalvo and H. D. Abruña, *Nano Lett.*, 2012, **12**, 5230–5238.
20 B. Zhang and D. S. Su, *Angew. Chem., Int. Ed.*, 2013, **52**, 8504–8506.
21 B. Zhang, W. Zhang, L. Shao and D. S. Su, *ChemCatChem*, 2013, **5**, 2586–2590.
22 B. Zhang, X. Ni, W. Zhang, L. Shao, Q. Zhang, F. Girgsdies, C. Liang, R. Schlogl and D. S. Su, *Chem. Commun.*, 2011, **47**, 10716–10718.
23 B. Zhang, D. Wang, W. Zhang, D. S. Su and R. Schlögl, *Chem. – Eur. J.*, 2011, **17**, 12877–12881.
24 B. Zhang and D. S. Su, *C. R. Phys.*, 2014, **15**, 258–268.
25 D. S. Su, B. Zhang and R. Schlögl, *Chem. Rev.*, 2015, **115**, 2818–2882.
26 W. Zhang and W. T. Zheng, *Phys. Chem. Chem. Phys.*, 2015, **17**, 14461–14469.
27 C. Cui, L. Gan, H.-H. Li, S.-H. Yu, M. Heggen and P. Strasser, *Nano Lett.*, 2012, **12**, 5885–5889.
28 P. Strasser, S. Koh, T. Anniyev, J. Greeley, K. More, C. Yu, Z. Liu, S. Kaya, D. Nordlund, H. Ogasawara, M. F. Toney and A. Nilsson, *Nat. Chem.*, 2010, **2**, 454–460.
29 A. B. A. A. Nassr, I. Sinev, M.-M. Pohl, W. Grünert and M. Bron, *ACS Catal.*, 2014, **4**, 2449–2462.
30 S. M. M. Ehteshami and S. H. Chan, *Electrochim. Acta*, 2013, **93**, 334–345.
31 Z. Liu, X. Y. Ling, X. Su and J. Y. Lee, *J. Phys. Chem. B*, 2004, **108**, 8234–8240.
32 H. Liao, A. Fisher and Z. J. Xu, *Small*, 2015, **11**, 3221–3246.
33 R. Ferrando, J. Jellinek and R. L. Johnston, *Chem. Rev.*, 2008, **108**, 845–910.
34 A. S. Shirinyan and M. Wautelet, *Nanotechnology*, 2004, **15**, 1720.
35 J. Greeley and M. Mavrikakis, *Nat. Mater.*, 2004, **3**, 810–815.
36 A. V. Ruban, H. L. Skriver and J. K. Nørskov, *Phys. Rev. B: Condens. Matter Mater. Phys.*, 1999, **59**, 15990–16000.
37 C. Cui, M. Ahmadi, F. Behafarid, L. Gan, M. Neumann, M. Heggen, B. R. Cuenya and P. Strasser, *Faraday Discuss.*, 2013, **162**, 91–112.
38 L. O. Paz-Borbón, R. L. Johnston, G. Barcaro and A. Fortunelli, *J. Chem. Phys.*, 2008, **128**, 134517.
39 L.-L. Wang and D. D. Johnson, *J. Am. Chem. Soc.*, 2009, **131**, 14023–14029.
40 G. Wang, M. A. Van Hove, P. N. Ross and M. I. Baskes, *J. Chem. Phys.*, 2005, **122**, 024706.
41 H. H. Hwu, J. Eng and J. G. Chen, *J. Am. Chem. Soc.*, 2002, **124**, 702–709.
42 K. J. J. Mayrhofer, V. Juhart, K. Hartl, M. Hanzlik and M. Arenz, *Angew. Chem., Int. Ed.*, 2009, **48**, 3529–3531.
43 Y. Gauthier, M. Schmid, S. Padovani, E. Lundgren, V. Buš, G. Kresse, J. Redinger and P. Varga, *Phys. Rev. Lett.*, 2001, **87**, 036103.
44 S. Y. Hwang, M. Zhang, C. Zhang, B. Ma, J. Zheng and Z. Peng, *Chem. Commun.*, 2014, **50**, 14013–14016.
45 C. Cui, L. Gan, M. Neumann, M. Heggen, B. Roldan Cuenya and P. Strasser, *J. Am. Chem. Soc.*, 2014, **136**, 4813–4816.

